RSC Advances

PAPER

View Article Online
View Journal | View Issue

Cite this: *RSC Adv.*, 2021, **11**, 2020

Low temperature scintillation performance of a Br-doped $CH_3NH_3PbCl_3$ single-crystalline perovskite

Jun Liu,[a] Dongwei Hei,[a] Qiang Xu,[*b] Xinjian Tan,[a] Jinlu Ruan,[a] Xiaoping Ouyang,[*ab] Jing Nie,[b] Kun Wei,[a] Qing Xu[a] and Bin Sun[a]

Received 9th August 2020
Accepted 17th October 2020

DOI: 10.1039/d0ra06860h

rsc.li/rsc-advances

Time response and light yield are two of the most important features of a scintillation detector, and are mostly determined by the luminescence properties of the scintillator. Here we have investigated the radioluminescence (RL) characteristics of a single-crystalline hybrid lead halide perovskite at both room temperature and low temperature. A dual-channel single photon correlation (DCSPC) system with a vacuum chamber is employed for the measurement. A rise time faster than 100 ps and several times enhancement of the crystal scintillation performances at low temperature have been observed. These behaviors demonstrated that bulk solution-grown single crystals of hybrid lead halide perovskites ($MAPbCl_3$ and Br-doped $MAPbBr_{0.08}Cl_{2.92}$, where MA = CH_3NH_3) can serve as stable scintillating materials for pulsed gamma detectors. In addition, this work provides a pathway for perovskite application and also attracts attention to investigating low-temperature scintillators.

1. Introduction

Pulsed gamma-ray detection is crucial for nuclear facility diagnosis, industrial inspection, and scientific research.[1–4] Both time response and sensitivity of the detector are the underlying physical properties that can extremely limit the scope of application and also commonly represent its ability to detect fast low-intensity gamma pulses.[5,6] However, most of the conventional scintillating materials suffer from some problems, such as low energy deposition efficiency (due to low atomic number), limitations of timing resolution, large size, unstable performance and so on.[7] Currently, low light yield together with slow rise time and decay time of scintillators are the key limitations towards fast gamma detection. Thus, it is worth finding another novel high-Z single crystal with fast time resolution for pulsed gamma-ray detection applications.[8]

Recently, organic–inorganic methylammonium lead halide single-crystalline materials ($MAPbX_3$, where MA = CH_3NH_3, X = Cl, Br or I) with perovskite structures have been presented during the past a few years and have attracted considerable attention.[9] Due to the good tolerance of optical and electronic characteristics, a lot of investigations were focusing on single crystal preparation, optical and electrical properties characterization.[10,11] Furthermore, because of X-ray and gamma ray energy deposition is proportional to the atomic number of the material, $MAPbX_3$ single crystals were reported aiming at the applications of pulsed X-ray or gamma ray detection.[12,13] For ionization radiation detection, the time response of direct photon-to-current conversion pulsed gamma ray detector has reached to μs for a bulk perovskite optoelectronic device.[14] The photon-to-current conversion scintillation of perovskite also has been investigated, which exhibits tunable light emission and nanosecond scintillation decay time. However, the relatively low light yield is not enough to be realized by the commercial utilization yet.

Many other scintillation semiconductor materials have shown very different behaviours at low temperatures due to the change of carrier generation and recombination dynamics.[15–18] Therefore, in this work, we explored the possibility of improving the light yield by operating at low temperatures in a high-vacuum chamber, focusing on the practical application of these promising $MAPbX_3$ materials and their compounds in scintillation detectors for pulsed gamma ray detection. Br-doped $MAPbCl_3$ single-crystalline materials ($MAPbCl_3$ and $MAPbBr_{0.08}Cl_{2.92}$) have been successfully synthesized at room temperature. We measured their radioluminescence (RL) temporal profiles by a dual-channel single photon correlation (DCSPC) system, with the cooler terminal in a vacuum chamber. Remarkable improvements on light yields and time resolutions (τ_{rise} < 100 ps) have been demonstrated under low temperature conditions.

2. Experimental

High-quality $MAPbCl_3$ and $MAPbBr_{0.08}Cl_{2.92}$ single crystals (SCs) were synthesized by using the inverse temperature crystallization growth method. The different molar ratio of CH_3NH_3Cl, $PbCl_2$ and $PbBr_2$ were dissolved into dimethylsulfoxide

[a]*State Key Laboratory of Intense Pulsed Radiation Simulation and Effect, Northwest Institute of Nuclear Technology, Xi'an 710024, China. E-mail: xuqiangxmu@nuaa.edu.cn*

[b]*Department of Nuclear Science and Technology, Nanjing University of Aeronautics and Astronautics, Nanjing 211106, China*

and N–N, dimethylformamide by using as precursor solution. Then, this precursor solution was kept at 80 °C for several days to gradually grow high-quality crystals. The process details have been reported in our previous publications.[19,20]

The dual-channel single photon correlation (DCSPC) method needs to employ two single photon detectors to detect random single photons of the sample. The distribution of the time interval between the arrival times of the two detectors describes the autocorrelation function of the fluorescence temporal profile.[21] A conventional dual-channel single photon correlation (DCSPC) system with a liquid helium cooling terminal and a vacuum chamber is employed to study the scintillation processes, which can provide low temperature down to 30 K and high measuring resolution of about 46 ps (calibrated by the Cerenkov luminescence).[21] And the function of ORTEC 9327 integrates the functions of ORTEC 9306 and ORTEC 9307. Two single photon detectors were used to count random emission photons. The time interval distribution represents the auto-correlation function of the fluorescence temporal profile. A schematic diagram of the experiment is shown in Fig. 1. The $MAPbX_3$ crystals are put on the face of the cooler terminal, in which four temperature probes are distributed. The excitation source is a radioisotope source ^{241}Am with an activity of about 103 Bq and at the energy of 5.48 MeV. Two ultrafast micro-channel-plate photomultiplier tubes (MCP-PMT, R3809U-50) are used to collect scintillation photons, which can provide a high gain about 105 and a fast timing precision. And the two MCP-PMTs have different distances from the $MAPbX_3$ sample, which makes sure one of the MCP-PMTs to receive only one photon at a time. The "start" and "stop" timing signals are given as $T_0 + t_1$ and $T_0 + t_2$, where T_0 is the reference time from the interaction of α with the sample, while t_1 and t_2 are the time spans for the two light signals transmitting to MCP-PMTs, respectively. A vacuum chamber is put in the dark box to provide a stable condition for the crystals, which is also needed by the cooler. The time range of the measurement system is 50 ns, which is corresponding to the MCA channel of 2048.

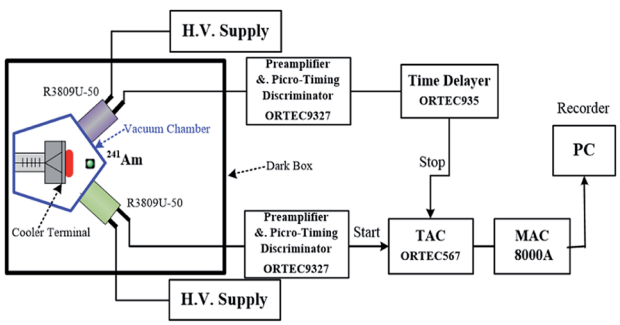

Fig. 1 The experimental schematic. The luminescence is excited with a radioisotope source ^{241}Am. Signals from two MCP-PMTs are amplified and discriminated (ORTEC 9327) to provide the "start" and "stop" timing signals of a time-to-amplitude converter (TAC, ORTEC 567). Then the distribution of time interval is recorded by a multi-channel analyzer (MCA8000A, AmpTek).

3. Results and discussion

Fig. 2 shows the single crystal XRD patterns of MAPbCl3 and $MAPbBr_{0.08}Cl_{2.92}$. Two diffraction peaks assigned to (002) and (221) have been observed, which exhibit a slight shifting to small angles after Br doped. This behavior indicates the Br is successfully doped into the lattice. The molar ratio of Br to Cl could be estimated by Vegard's law based on the peak shifts.[22]

In addition, we have developed X-ray fluorescence (XRF) spectroscopy measurement to test the actual molar ratio of Br to Cl.[23] Fig. 3 shows a clear and strong peak locating at 11.9 keV that ascribed to Br Kα1 of the XRF spectra. The calculated molar ratio of Br to Cl is about 0.08 to 2.92, which is consistent with the above theoretically calculated results.

Luminescence time characteristics of Br-doped $MAPbCl_3$ crystals are evaluated at room temperature. As is shown in Fig. 4, the scintillation properties of $MAPbCl_3$ and $MAPbBr_{0.08}Cl_{2.92}$ single crystals are very different. The luminescence temporal profile of $MAPbCl_3$ crystal indicates that the rise time is about 1.1 ns and the full width of half maximum (FWHM) is about 1.35 ns. The decay curve can be fitted with single exponential function:[24]

$$f(t) = y_0 + A_1 \exp[-(t - t_0)/\tau_1],$$

where y_0 and t_0 are the background, A_1 is the amplitude and τ_1 is the decay time. The decay time constant of $MAPbBr_{0.08}Cl_{2.92}$ crystal is about 1.01 ns at room temperature, which indicates that the profile exhibits Gaussian distribution. The rise time, the FWHM and the decay time constant of $MAPbBr_{0.08}Cl_{2.92}$ crystal are about 1.43 ns, 2.91 ns and 1.27 ns respectively, which displays slower luminescence time than $MAPbCl_3$ crystal. In addition, the amplitudes of two temporal profiles are similar, which illustrates that their light yields are similar too. However, it is also found that the decay curve of $MAPbBr_{0.08}Cl_{2.92}$ crystal can be well fitted by one exponential function with the iteration algorithm of orthogonal distance regression, which is different from that for pure $MAPbCl_3$ sample. It indicates that the luminescence kinetics of Br-doped sample may contain slow components introduced by Br doping. These behaviours are indicators of a slower process in the recombination dynamics.[20]

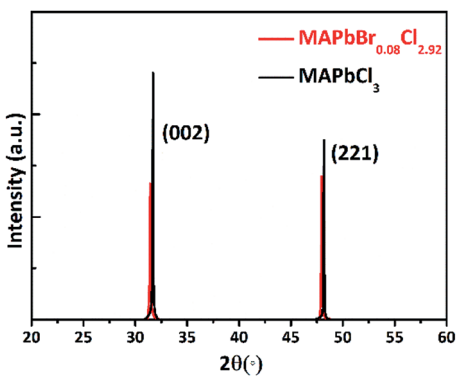

Fig. 2 Single crystal single crystal XRD pattern of bulk MAPbCl3 and $MAPbBr_{0.08}Cl_{2.92}$.

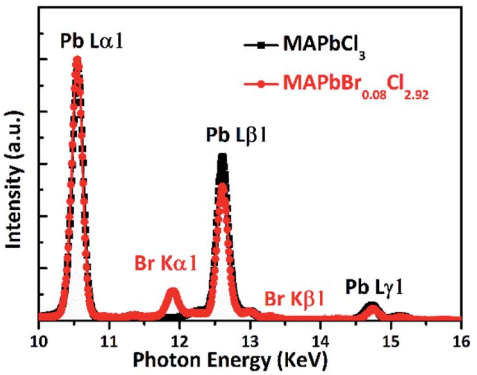

Fig. 3 XRF data of bulk $MAPbCl_3$ and $MAPbBr_{0.08}Cl_{2.92}$.

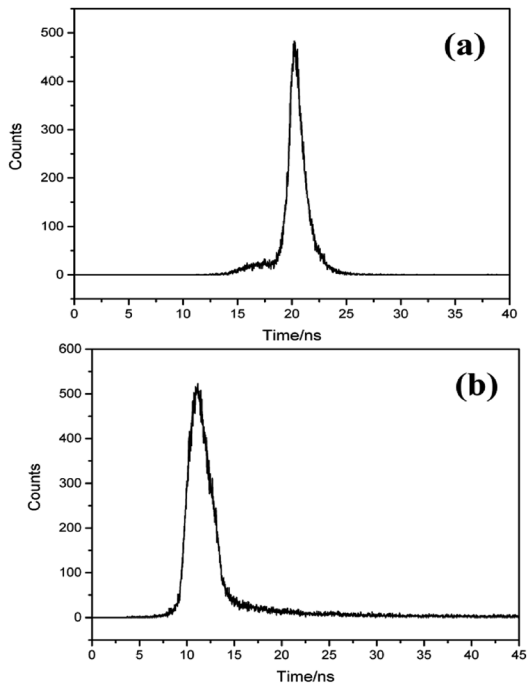

Fig. 4 Time response profiles of $MAPbX_3$ scintillators at room temperature. (a) Decay curve of $MAPbCl_3$ crystals perfectly fitted by single exponential function with the iteration algorithm of Levenberg Marquardt. (b) Decay curve of $MAPbBr_{0.08}Cl_{2.92}$ crystals fitted by single exponential function with the iteration algorithm of orthogonal distance regression.

Luminescence characteristics of Br-doped $MAPbCl_3$ crystals were measured under the same condition except the temperature of cooler terminal. The scintillation time profile of Br-doped $MAPbCl_3$ crystals at 30 K is shown in Fig. 5. The scintillation decay time is perfectly fitted by two exponential function:

$$f(t) = y_0 + A_1 \exp(-t/\tau_1) + A_2 \exp(-t/\tau_2).$$

The fast time constant τ_1 and slow decay time constant τ_2 are 2.4 ns and 5.26 ns, respectively, which indicate that carriers recombination dynamics undergo a slower process at cooling temperature. The temperature dependence of the luminescence

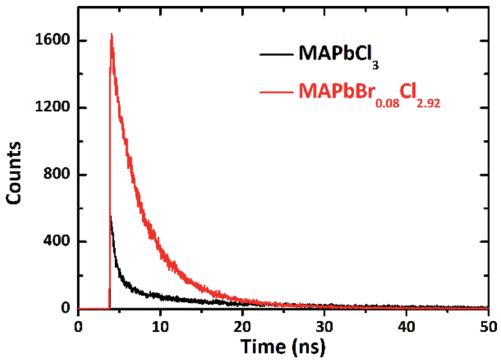

Fig. 5 Time response profile of $MAPbCl_3$ and $MAPbBr_{0.08}Cl_{2.92}$ scintillators at low temperature of 30 K, excited with alpha particles.

decay in both channels by considering the dynamics of radiative and non-radiative transition between the excited and ground states of the emission center, which correlates well with the conclusions from photoluminescence decay studies of $MAPbX_3$ below 77 K.[25] Worthwhile to be noticed that the amplitude of the scintillation profile at 30 K grows up to about three times higher than that at room temperature. The increased light yield with cooling is mainly introduced by the recombination of extra free and bound excitons due to their strong temperature dependence.[26]

Importantly, the rise time of the time response profile turns to be much faster at 30 K, which is over the time resolution ability of the DCSPC system. Since the time resolution of the measuring system is about 46 ps, which has been calibrated by the Cherenkov light produced with the quartz glass irradiated by gamma-rays. And the light spectrum is not the same as that in this work, there will be little disparity error resulted from optical dispersion. The error is usually less than 10 ps, because the optical path difference of 10 mm (very large for this measurement) can only cause a gap of about 33 ps. Conservatively, we believe that τ_{rise} is shorter than 100 ps according to the curve. In this case, the time performance of $MAPbCl_3$ crystal scintillation is largely improved at low temperature, though the decay time gets slower to a tolerable level. The results reveal that $MAPbCl_3$ crystal can be used to detect a pulsed ultra-fast gamma ray with a lower intensity.

The scintillation pulse of Br-doped $MAPbBr_{0.08}Cl_{2.92}$ crystal has also been investigated in the same condition. The time response profile of $MAPbBr_{0.08}Cl_{2.92}$ is obtained and the result is shown in Fig. 5 (red curve). Compared with the results at room temperature, the light yield exhibits an obvious enhancement, and the counting rate is high enough to make the waveform smooth. The accurate value of its rising edge time is also over the measuring resolution of the DCSPC system, and the slow component of the decay curves becomes more pronounced. The scintillation decay curve of $MAPbBr_{0.08}Cl_{2.92}$ crystals at 30 K is perfectly fitted by two exponential functions:

$$f(t) = y_0 + A_1 \exp(-t/\tau_1) + A_2 \exp(-t/\tau_2).$$

The fast time constant is $\tau_1 = 0.74$ ns and the slow time constant is $\tau_2 = 8.39$ ns. The FWHM of the response profile is decreased to about 683 ps, which indicates that the luminescence dynamics is dominated by the fast recombination processes due to deep level transitions and more defect centers at 30 K. However, the amplitude decreases by about three times than pure $MAPbCl_3$ crystal at the same temperature, which is an indication of more carriers undergoing non-radiative recombination processes due to more traps. The slow component is mainly attributed to the trapping and release of charge carriers as expected.[27,28] These features show that the scintillation response of $MAPbBr_{0.08}Cl_{2.92}$ crystals is faster than that of $MAPbCl_3$ crystals, while the light yield of $MAPbBr_{0.08}Cl_{2.92}$ crystals is relatively lower than that of undoped $MAPbCl_3$ crystals.[20]

In addition, as shown in Fig. 6, we have measured the RL spectra under low temperature, which was excited by 40 keV X-ray from a portable X-ray tube. The RL spectra are different when the temperature is lower and higher than 150 K. This phenomenon may be linked to the phase transition process from the orthorhombic phase to the cubic phase with the rising of temperature.[29,30] While the temperature is under 150 K, three peaks have been observed. The high-energy peak centered at 387 nm is attributed to free exciton recombination emission. Emission peak located at 400 nm is mainly ascribed to near bound exciton emission.[31] Low energy emission peak at 415 nm is originally from the excitonic transition.[18,32] In addition, we have calculated exciton binding energy by using the relationship between the light emission intensity and temperature:[33]

$$I(T) = \frac{I_0}{1 + A e^{-E_B/k_B T}}$$

.where $I(T)$ is the RL intensity, T is temperature, I_0 is the RL intensity at 0 K, E_B the exciton binding energy, and k_B the Boltzmann constant, and A is a fitting parameter. The calculated exciton binding energy is about 23.2 meV and 28.5 meV, respectively. All these results are greatly matching with our previous study. This behavior indicated that orthorhombic phase Br-doped $MAPbCl_3$ crystals at low temperatures (<150 K) could be utilized as a relatively high light yield and fast gamma-ray detector.

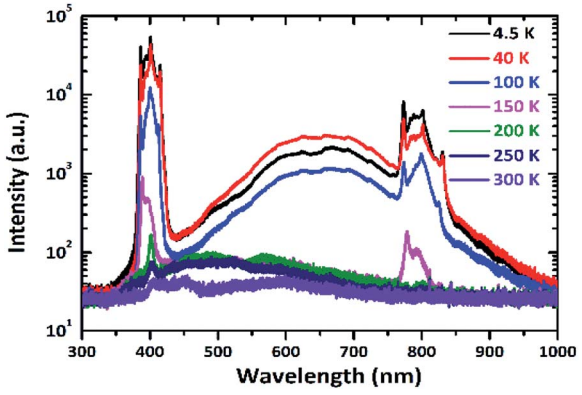

Fig. 6 Temperature-dependent RL spectra of $MAPbCl_3$ crystals excited with 40 keV monoenergetic X-ray.

4. Conclusions

In summary, we have synthesized Br-doped $MAPbCl_3$ single-crystalline materials by using an inverse temperature crystallization growth method. The time response profiles show that light yield and time resolution (especially the rise time) have been remarkably improved under low temperatures. In addition, the time response profiles at low temperatures also display different decay curves compared with those at room temperature, which indicates that luminescence kinetics in Br-doped $MAPbCl_3$ exhibit significant changes. The results provide a path to improve the light yield and solve the deliquescence by operating at low temperatures in high-vacuum chamber. The changes at low temperatures may guide the practicable application of the Br-doped $MAPbCl_3$ single crystals and their compounds as promising scintillation materials for fast gamma ray detectors.

Conflicts of interest

There are no conflicts to declare.

Acknowledgements

This work was funded by the National Natural Science Foundation of China (Grant No. 11905173).

References

1 M. Danielsson, P. Fonte, T. Francke, C. Iacobaeus, J. Ostling and V. Peskov, *Nucl. Instrum. Methods Phys. Res., Sect. A*, 2004, **518**, 406.
2 S. Li, B. Shen, J. Xu, T. Xu, Y. Yu, J. Li, X. Lu, C. Wang, X. Wang, X. Liang, Y. Leng, R. Li and Z. Xu, *Phys. Plasmas*, 2017, **24**, 093104.
3 A. Benedetti, M. Tamburini and C. H. Keitel, *Nat. Photonics*, 2018, **12**, 319.
4 X.-L. Zhu, M. Chen, T.-P. Yu, S.-M. Weng, L.-X. Hu, P. McKenna and Z.-M. Sheng, *Appl. Phys. Lett.*, 2018, **112**, 174102.
5 F. Foulon, B. Brullot, C. Rubbelynck, P. Bergonzo and T. Pochet, *IEEE Trans. Nucl. Sci.*, 1996, **43**, 1372.
6 L. Liu, X. Ouyang, J. Zhang, X. Zhang and Y. Zhong, *AIP Adv.*, 2014, **4**, 017114.
7 M. Moszyński, A. Syntfeld-Każuch, L. Swiderski, M. Grodzicka, J. Iwanowska, P. Sibczyński and T. Szczęśniak, *Nucl. Instrum. Methods Phys. Res., Sect. A*, 2016, **805**, 25.
8 N. J. Cherepy, G. Hull, A. D. Drobshoff, S. A. Payne, E. van Loef, C. M. Wilson, K. S. Shah, U. N. Roy, A. Burger, L. A. Boatner, W.-S. Choong and W. W. Moses, *Appl. Phys. Lett.*, 2008, **92**, 083508.
9 Y. Liu, Z. Yang, D. Cui, X. Ren, J. Sun, X. Liu, J. Zhang, Q. Wei, H. Fan, F. Yu, X. Zhang, C. Zhao and S. F. Liu, *Adv. Mater.*, 2015, **27**, 5176.
10 C. Eames, J. M. Frost, P. R. F. Barnes, B. C. O'Regan, A. Walsh and M. S. Islam, *Nat. Commun.*, 2015, **6**, 7497.

11 J.-P. Correa-Baena, M. Saliba, T. Buonassisi, M. Grätzel, A. Abate, W. Tress and A. Hagfeldt, *Science*, 2017, **358**, 739.
12 S. Kishimoto, K. Shibuya, F. Nishikido, M. Koshimizu, R. Haruki and Y. Yoda, *Appl. Phys. Lett.*, 2008, **93**, 261901.
13 Q. Xu, W. Shao, Y. Li, H. Zhang, X. Ouyang, X. Zhang, J. Nie, X. Ouyang and B. Liu, *J. Alloys Compd.*, 2019, **810**, 151896.
14 Q. Xu, W. Shao, Y. Li, X. Zhang, X. Ouyang, J. Liu, B. Liu, Z. Wu, X. Ouyang, X. Tang and W. Jia, *ACS Appl. Mater. Interfaces*, 2019, **11**, 9679.
15 B. Globisch, R. J. B. Dietz, D. Stanze, T. Göbel and M. Schell, *Appl. Phys. Lett.*, 2014, **104**, 172103.
16 X. A. Cao, S. F. LeBoeuf, L. B. Rowland, C. H. Yan and H. Liu, *Appl. Phys. Lett.*, 2003, **82**, 3614.
17 Y.-C. Lin, M.-J. Tasi, W.-C. Chou, W.-H. Chang, W.-K. Chen, T. Tanaka, Q. Guo and M. Nishio, *Appl. Phys. Lett.*, 2013, **103**, 261905.
18 C. Wehrenfennig, M. Liu, H. J. Snaith, M. B. Johnston and L. M. Herz, *APL Mater.*, 2014, **2**, 081513.
19 Q. Xu, W. Shao, X. Zhang, J. Liu, X. Ouyang, X. Tang and W. Jia, *J. Alloys Compd.*, 2019, **792**, 185.
20 Q. Xu, W. Shao, J. Liu, Z. Zhu, X. Ouyang, J. Cai, B. Liu, B. Liang, Z. Wu and X. Ouyang, *ACS Appl. Mater. Interfaces*, 2019, **11**, 47485.
21 L. Chen, J. Ruan, M. Xu, S. Yi, J. Hu, Z. Zhang, J. Liu and X. Ouang, *Nucl. Instrum. Methods Phys. Res.*, 2019, **933**, 71.
22 J. H. Noh, S. H. Im, J. H. Heo, T. N. Mandal and S. I. Seok, *Nano Lett.*, 2013, **13**, 1764–1769.
23 Q. Shan, X. Zhang, Y. Zhang, W. Jia, Y. Ling, D. Hei and S. Chu, *Spectrosc. Lett.*, 2016, **49**, 188–193.
24 S. A. Hashemizadeh, J.-P. R. Wells, P. Murzyn, J. Brown, B. D. Jones, T. Wang, P. J. Parbrook, A. M. Fox, D. J. Mowbray and M. S. Skolnick, *Appl. Phys. Lett.*, 2005, **87**, 232106.
25 Y. Liu, H. Lu, J. Niu, H. Zhang, S. Lou, C. Gao, Y. Zhan, X. Zhang, Q. Jin and L. Zheng, *AIP Adv.*, 2018, **8**, 095108.
26 K. Wu, A. Bera, C. Ma, Y. Du, Y. Yang, L. Lib and T. Wu, *Phys. Chem. Chem. Phys.*, 2014, **16**, 22476.
27 Y. Li, W. Shao, X. Ouyang, Z. Zhu, H. Zhang, X. Ouyang, B. Liu and Q. Xu, *J. Phys. Chem. C*, 2019, **123**, 17449.
28 H. Diab, C. Arnold, F. Lédée, G. Trippé-Allard, G. Delport, C. Vilar, F. Bretenaker, J. Barjon, J.-S. Lauret, E. Deleporte and D. Garrot, *J. Phys. Chem. Lett.*, 2017, **8**, 2977.
29 F. Brivio, J. M. Frost, J. M. Skelton, A. J. Jackson, O. J. Weber, M. T. Weller, A. R. Goñi, A. M. A. Leguy, P. R. F. Barnes and A. Walsh, *Phys. Rev. B: Condens. Matter Mater. Phys.*, 2015, **92**, 144308.
30 P. Sadhukhan, A. Pradhan, S. Mukherjee, P. Sengupta, A. Roy, S. Bhunia and S. Das, *Appl. Phys. Lett.*, 2019, **114**, 131102.
31 H.-H. Fang, R. Raissa, M. Abdu-Aguye, S. Adjokatse, G. R. Blake, J. Even and M. A. Loi, *Adv. Funct. Mater.*, 2015, **25**, 2378.
32 J. Xing, X. F. Liu, Q. Zhang, S. T. Ha, Y. W. Yuan, C. Shen, T. C. Sum and Q. Xiong, *Nano Lett.*, 2015, **15**, 4571.
33 T. J. Savenije, C. S. Ponseca, L. Kunneman, M. Abdellah, K. Zheng, Y. Tian, Q. Zhu, S. E. Canton, I. G. Scheblykin, T. Pullerits, A. Yartsev and V. Sundström, *J. Phys. Chem. Lett.*, 2014, **5**, 2189.